

Journal of Materials Chemistry A

Accepted Manuscript



This is an *Accepted Manuscript*, which has been through the Royal Society of Chemistry peer review process and has been accepted for publication.

Accepted Manuscripts are published online shortly after acceptance, before technical editing, formatting and proof reading. Using this free service, authors can make their results available to the community, in citable form, before we publish the edited article. We will replace this *Accepted Manuscript* with the edited and formatted *Advance Article* as soon as it is available.

You can find more information about *Accepted Manuscripts* in the [Information for Authors](#).

Please note that technical editing may introduce minor changes to the text and/or graphics, which may alter content. The journal's standard [Terms & Conditions](#) and the [Ethical guidelines](#) still apply. In no event shall the Royal Society of Chemistry be held responsible for any errors or omissions in this *Accepted Manuscript* or any consequences arising from the use of any information it contains.

ARTICLE

Synthesis of SiO₂ nanofibre confined Ni catalyst by electrospinning for CO₂ reforming of methane

Cite this: DOI: 10.1039/x0xx00000x

Shipeng Wen,^{ab} Meili Liang,^{ab} Junma Zou,^{ab} Sun Wang,^{ab} Xiandong Zhu,^{ab} Li Liu^{ab} and Zhou-jun Wang^{*ab}Received 00th March 2015,
Accepted 00th March 2015

DOI: 10.1039/x0xx00000x

www.rsc.org/

Silica (SiO₂) nanofibre confined nickel (Ni) catalyst has been successfully synthesized by the electrospinning technique and systematically characterized with thermogravimetric/differential thermal analysis (TG/DTA), X-ray photoelectron spectroscopy (XPS), N₂ sorption, X-ray diffraction (XRD), scanning electron microscopy (SEM), high resolution-transmission electron microscopy (HR-TEM), temperature-programmed oxidation (O₂-TPO), temperature-programmed reduction (H₂-TPR) and temperature-programmed desorption (CO₂-TPD) measurements. In the electrospinning synthesized Ni/SiO₂ catalyst, most of the Ni nanoparticles were confined inside SiO₂ nanofibres with average particle size of 8.1 nm. Compared with the Ni/SiO₂ catalyst conventionally prepared via incipient impregnation method using commercial SiO₂ powder as the support, the electrospun Ni/SiO₂ catalyst exhibits improved metal dispersion and enhanced metal-support interaction, leading to slightly higher activity and much better stability in carbon dioxide (CO₂) reforming of methane. Carbon deposition, rather than metal sintering, is identified as the main cause for the deactivation of Ni/SiO₂ catalyst under current conditions. The present work demonstrates that electrospinning is a potential technique for the fabrication of nanoconfined catalysts with superior catalytic performance and macro-scale handling properties.

Introduction

Energy crisis and environment pollution have been recognized as two of most pressing problems for human beings.^{1,2} The continuous consumption of fossil fuels led to depletion of energy resources as well as accumulation of greenhouse gases. Converting the greenhouse gases into clean energy has been one of the grand challenges all over the world.³ In this regard, carbon dioxide reforming (CO₂) reforming of methane becomes a promising technology due to its environmental benefit from utilizing two potent greenhouse gases and clean energy supply from producing valuable synthesis gas for fuel synthesis.^{4,5} Although considerable efforts have been devoted on this technology in the last decades, industrial application is still not realized. The prime bottleneck for industrialization is the catalyst. Considering the cost and availability, non-noble metal catalysts, particularly Ni-based catalysts, are regarded as the most promising candidate due to their excellent activity. However, Ni-based catalysts always suffer from rapid deactivation because of

carbon deposition and/or metal sintering at elevated operating temperature.^{6,7} Therefore, it is critical to develop Ni-based catalysts with better stability.

Previous results revealed that nano-morphology of the metal or support may affect the catalytic performance of the catalysts in CO₂ reforming of methane.^{8,9} Recently, more and more work have demonstrated that nanoconfined catalysts deliver exceptional activity and stability.⁸⁻¹⁶ For example, He *et al.*¹⁴ reported that nanocatalysts with layered double hydroxides as precursors/supports can afford superior catalytic performance and recyclability due to the confinement effects of the lamellar structure. Zhang *et al.*¹⁵ synthesized nonoconfined nickel polysilicate nanotubes catalyst which exhibited enhanced anti-sintering and -coke properties. Xie and co-workers¹⁶ immobilized Ni nanoparticles into the uniform channels of mesoporous silica and obtained confined catalyst with improved catalytic performances. Du and co-workers^{17,18} fabricated confined Ni catalysts with various methods, yielding catalysts with enhanced coke- and sintering-resistance. In a word,

prospective results have been acquired by design of nanoconfined catalysts. However, synthesis of nanoconfined catalysts in a scalable manner still remains challenging.

Electrospinning is a technique widely used in polymer-based fibre industry that utilizes high electrostatic force to fabricate fibres with controllable diameter ranging from nano- to micron-meter scale. The advantage of electrospinning is that the process can be realized in a continuous way with scale-up potential due to its simplicity, versatility, low cost, high yield and excellent reproducibility.^{19,20} Moreover, a number of recent work have revealed that *in situ* formed metal nanoparticles (Au, Co, etc.) are well distributed inside the electrospun nanofibres (TiO₂, C, etc.), exhibiting high performance in photoanode, Li-ion batteries, solar cell, electromagnetic wave absorbers and so on.²¹⁻²⁵ That is, confinement effect may exist in the electrospun nanofibre composite. Electrospinning may serve as a scalable technique to synthesize nanoconfined catalysts.

Previously we have employed electrospinning technique to synthesize SiO₂ nanofibres with the average diameter in the range of 200-500 nm.²⁶ Herein, SiO₂ nanofibre confined Ni catalyst was synthesized and the obtained Ni/SiO₂ catalyst was tested in CO₂ reforming of methane to confirm the potential confinement effect. The catalysts were characterized with thermogravimetric/differential thermal analysis (TG/DTA), X-ray photoelectron spectroscopy (XPS), N₂ sorption, X-ray diffraction (XRD), scanning electron microscopy (SEM), high resolution-transmission electron microscopy (HR-TEM), temperature-programmed oxidation (O₂-TPO), temperature-programmed reduction (H₂-TPR) and temperature-programmed desorption (CO₂-TPD) measurements.

Experimental

Catalyst synthesis

As shown in Fig. 1, synthesis of SiO₂ nanofibre confined Ni catalyst includes the following steps: electrospinning, drying, and thermal calcination. The electrospinning setup and experimental protocol have been described in detail elsewhere.²⁶ The precursor for electrospinning consisted of three solution mixtures. 1.4 g polyvinyl pyrrolidone (PVP Sigma Aldrich; mol wt 1 300 000 g mol⁻¹) was dissolved in 5.0 g N,N-dimethylformamide (DMF, AR Grade) and 2.5 g dimethyl sulfoxide (DMSO, AR Grade) to prepare solution I. 5.2 g TEOS was mixed with 1.0 g hydrochloric acid (0.3 wt%) and 1.5 g absolute ethanol to prepare solution II. 0.83 g Ni(NO₃)₂·6H₂O (Sigma Aldrich) was dissolved in 1.0 g absolute ethanol to prepare solution III. After complete dissolution, the solutions of I, II and III were mixed together and magnetically stirred for 2 h. Subsequently, the resulting precursor was transferred into a plastic syringe for electrospinning process. The syringe had a 22-gauge stainless-steel needle with a blunt tip. The electrospinning setup included a high voltage power supply (Ormond Beach, model ES30P) and a laboratory-made roller (o.d. 25 cm). During electrospinning, the precursor was subjected to a high voltage of 15 kV. The distance between the tip and roller was fixed at 25 cm and the feeding rate was maintained at 1.0 ml h⁻¹. The electrospun composite was collected as overlaid nanofiber mats on an aluminum foil that covered the roller. The obtained sample was then kept under ambient condition for 12 h, followed by drying at 110 °C overnight. Finally, the sample was calcined at 800 °C for 4 h unless otherwise mentioned. The nickel amount was 10 wt%.

For the purpose of comparison, another two catalysts were conventionally prepared via incipient impregnation method.²⁷ One catalyst employed the commercial SiO₂ powder (Sigma Aldrich) as the support. The other catalyst employed electrospun SiO₂ nanofibre as the support. In the following sections, SiO₂ nanofibre confined catalyst was labelled as Ni/SiO₂-F, SiO₂ powder impregnated catalyst was labelled as Ni/SiO₂-C, and SiO₂ nanofibre impregnated catalyst was labelled as Ni/SiO₂-FI.

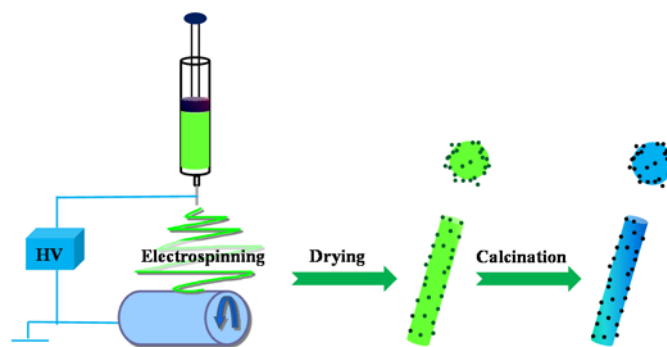


Fig. 1 Schematics for the synthesis of catalysts by electrospinning method.

Catalyst Characterizations

Thermogravimetric/differential thermal analysis (TG/DTA). TG/DTA measurements were performed on a Shimadzu DTG-60A thermal analyzer apparatus that allowed TG and DTA curves to be recorded simultaneously. The experiments were carried out from room temperature up to 800 °C at a heating rate of 10 °C min⁻¹ in an air flow (30 ml min⁻¹), using Al₂O₃ as a reference. 5-10 mg of sample was used for each measurement.

X-ray photoelectron spectroscopy (XPS). XPS spectra were acquired on an ESCALAB 250 (Thermo Electron Co.) spectrometer using a monochromated Al K α X-ray source (1 486.6 eV) and a hemispherical analyzer with pass energy of 30.0 eV. The binding energy was calibrated by the C 1s peak (285.0 eV) of the surface adventitious carbon.

N₂ sorption. N₂ adsorption-desorption isotherms were measured at -196 °C on a Sorptomatic 1990 instrument (Thermo Electron). Prior to measurement, the sample was outgassed at 300 °C for 6 h. Brumauer-Emmett-Teller (BET) method was employed to calculate the specific surface area. The pore volume and average pore diameter were calculated by Horvath-Kawazoe (H-K) method.

X-ray diffraction (XRD). XRD patterns were collected on a Rigaku D/MAX 2500VB 2+ /PC system using Cu K α radiation ($\lambda=0.154056$ nm) at a scanning speed of 10° min⁻¹ in the 2 θ range of 10 - 90°. The voltage was 40 kV and the current was 200 mA. The phase identification was made by comparing with Joint Committee on Powder Diffraction Standards (JCPDS).

Scanning electron microscopy (SEM). SEM images were recorded on a Hitachi S-4800 microscope. The working voltage was 5 kV. Prior to examinations, the specimen was sputter-coated with gold to avoid charge accumulations.

High resolution-transmission electron microscopy (HR-TEM). HR-TEM images were recorded on a Tecnai G2 F30 system (FEI Company, Hillsboro, OR) with Z-contrast imaging in the scanning TEM (STEM) mode. The working voltage was 300 kV. The powder sample was sonicated in ethanol for 10 min, dropped and dried on carbon-coated copper grids prior to test.

Temperature-programmed oxidation (O₂-TPO). O₂-TPO test was performed on a Micromeritics Autochem II 2920 catalyst characterization system connected to a mass spectrometer (QIC-20, Hiden Analytical Ltd.). The spent catalyst sample (about 50 mg) was heated in flowing 3% O₂/He (30 mL min⁻¹) over the temperature range of 50 - 1000 °C at a ramping rate of 10 °C min⁻¹. The m/z signals at 18, 28, 32 and 44 were continuously recorded. The results of the m/z = 44 (CO₂ signal) were shown in O₂-TPO profiles.

Temperature-programmed reduction (H₂-TPR). H₂-TPR test was performed on a Thermo Electron TPD/R/O 1100 series catalytic surface analyzer equipped with a thermal conductivity detector (TCD). The sample (about 0.1 g) was initially purged through heating in Ar gas (30 ml min⁻¹) from room temperature to 200 °C at a ramping rate of 10 °C min⁻¹ followed by a holding of 1 h to remove physically absorbed impurities on the catalyst surface. Then the catalyst was cooled down to 50 °C. H₂-TPR test was subsequently carried out by linearly increasing the temperature from 50 to 1000 °C at 10 °C min⁻¹ in a flow of 10% H₂/Ar mixture gas (30 ml min⁻¹).

Temperature-programmed desorption (CO₂-TPD). CO₂-TPD test was performed on the same facility used for H₂-TPR. The sample (about 0.1 g) was initially purged through heating in He gas (30 ml min⁻¹) from room temperature to 200 °C at a ramping rate of 10 °C min⁻¹ followed by a holding of 1 h to remove physically absorbed impurities on the catalyst surface. After the catalyst was cooled down to 50 °C, the samples were saturated with CO₂ for 1 h and flushed with He for 30 min to remove physisorbed CO₂. Subsequently, CO₂-TPD test was carried out by linearly increasing the temperature from 50 to 800 °C at 10 °C min⁻¹ in flowing He (30 ml min⁻¹).

Catalytic Testing

The prepared catalysts were tested at 700 °C under atmospheric pressure in CO₂ reforming of methane. Catalyst assessment was carried out in a fixed-bed vertical quartz reactor (i.d. 8 mm) with a central thermocouple to monitor the temperature of the catalyst bed. For each test, 100 mg of the catalyst (40 - 60 mesh) was packed on a quartz wool bed. The catalyst was pre-reduced *in situ* by flowing 40 ml min⁻¹ of H₂ at 500 °C for 2 h. The feed gases of CH₄, CO₂ and Ar with a ratio of 1:1:2 were introduced into the catalyst bed at a flow rate of 80 ml min⁻¹, corresponding to a gas hourly space velocity (GHSV) of 48 000 ml (h gcat)⁻¹. The feed gases at ultra-high pure grade (>99.999%) were used without further purification. The effluent gases from the reactor were analysed with an online gas chromatograph (GC Zhejiang Fuli Analytical Instrument Co. LTD; model 9790 II) equipped with a TCD using a Porapak Q packed column. An ice-cold trap was set between the reactor exit and the GC sampling valve to remove the water formed during reaction. Preliminary tests have confirmed that both the internal and external diffusion were completely eliminated under the current experimental conditions.

In the present work, the conversion of methane and CO₂ and the selectivity of H₂ and CO were calculated according to the following formulas:

$$X_{CH_4}\% = \frac{F_{CH_4, in} - F_{CH_4, out}}{F_{CH_4, in}} \times 100$$

$$X_{CO_2}\% = \frac{F_{CO_2, in} - F_{CO_2, out}}{F_{CO_2, in}} \times 100$$

$$S_{H_2}\% = \frac{F_{H_2, out}}{2[F_{CH_4, in} - F_{CH_4, out}]} \times 100$$

$$S_{CO}\% = \frac{F_{CO, out}}{[F_{CH_4, in} - F_{CH_4, out}] + [F_{CO_2, in} - F_{CO_2, out}]} \times 100$$

$$F_i = F_{total} \times C_i$$

where X , S and F represent conversion, selectivity and gas flow rate, respectively. C_i is the molar fraction of component i in the feed or effluent gases.

Results and discussion

Decomposition of precursor.

Compared with the conventional preparation strategy using commercial SiO₂ powder as the support via incipient impregnation method, the synthesis of SiO₂ nanofibre confined Ni catalyst via electrospinning method has a more complex precursor. Therefore, the decomposition of precursor should be examined first. Shown in Fig. 2 are the TG-DTG profiles of Ni/SiO₂-F composite after drying procedure. DTG profile clearly illustrates that four weight loss stages occurred during the calcination process. Similar TG results have been reported in the literature on the electrospun SiO₂ nanofibre.^{28,29} The first stage with DTG peak located at 68 °C could be ascribed to the desorption of moisture. The second stage with DTG peak at 203 °C could be attributed to the evaporation of trapped solvents (DMF and/or DMSO). The third stage with DTG peak at 368 °C corresponded to the decomposition of PVP. The last stage with DTG peak at 600 °C was assigned to the release of water formed from the condensation of hydrolysed TEOS in the silica nanofibre. TG-DTG results suggest that the calcination temperature for the synthesis of Ni/SiO₂-F catalyst should be higher than 600 °C.

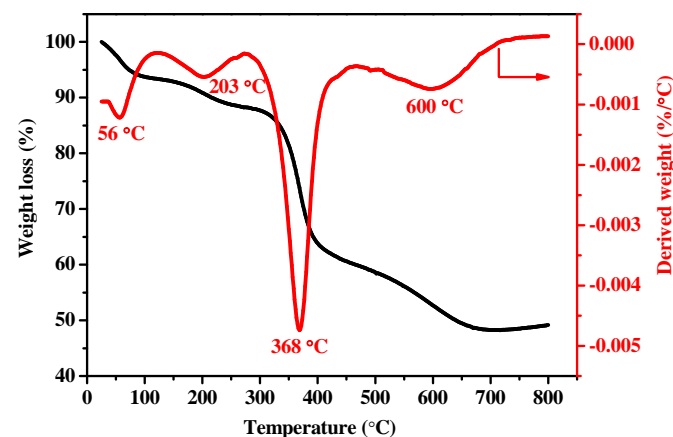


Fig. 2 TG-DTG profiles of Ni-SiO₂-F after drying procedure.

To further confirm the decomposition of precursor, XPS characterization was conducted to study the surface composition of the calcined Ni/SiO₂-F catalyst. Shown in Fig. S1a is the survey scan spectrum of Ni/SiO₂-F catalyst calcined at 600 °C, in which only Ni, Si, O and C elements were observed.³⁰ Since C element was from the adventitious contaminants, the survey scan spectrum suggests that most of the precursor was decomposed through calcination at 600 °C. However, high resolution scan reveals that limited N element still existed on the surface (Fig. S1b), which should be the residual fragment from

PVP.²⁹ Further increasing the calcination temperature up to 800 °C led to the complete elimination of N species.

Besides, the calcination effect of Ni/SiO₂-F catalysts has been tested in CO₂ reforming of methane. As illustrated in Fig. 3, the initial activity in terms of CH₄ conversion increased with calcination temperature in the range of 600-800 °C, which may be related to the gradual elimination of the N contaminants. Further increasing the calcination temperature to 900 °C resulted in a diminished initial activity, which may be related to the sintering of Ni nanoparticles at high temperature. Therefore, the optimal calcination temperature for the Ni/SiO₂-F catalyst is 800 °C. SEM images in Fig. S2 shows the morphology of the Ni/SiO₂-F catalyst before and after calcination at 800 °C, in which nanofibres with diameter in the range of 200-500 nm were observed.

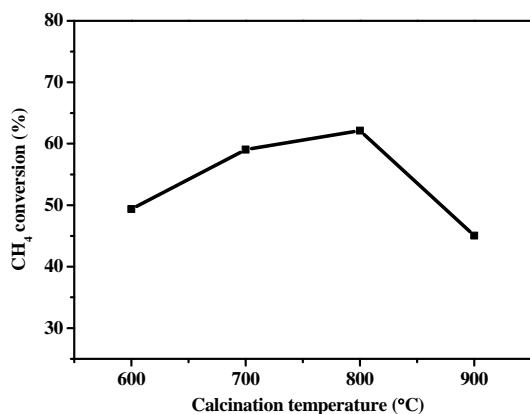


Fig. 3 Initial activity for CO₂ reforming of methane over the Ni/SiO₂-F catalyst as a function of calcination temperature. Reaction conditions: P=1 atm; T=700 °C; the nickel amount=10 wt%; CH₄:CO₂:Ar=1:1:2; GHSV=48 000 ml (h gcat)⁻¹.

Furthermore, the porosity of the calcined Ni/SiO₂-F catalyst was characterized by N₂ sorption. As shown in Fig. 4, a type I isotherm was observed, typical for materials mainly consisted of micropores. The BET surface area was 271.8 m² g⁻¹. The micropore volume and average pore diameter calculated by the H-K method were 0.12 cm³ g⁻¹ and 0.48 nm, respectively. N₂ sorption results suggest that the electrospinning synthesized Ni/SiO₂-F catalyst possessed sufficient micropores, suitable for catalytic applications.

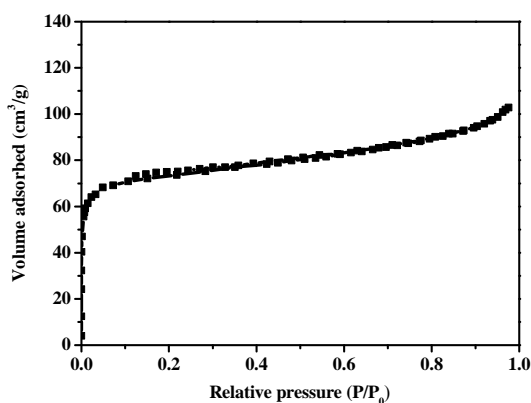


Fig. 4 N₂ adsorption-desorption isotherms of the Ni/SiO₂-F catalyst after calcination at 800 °C.

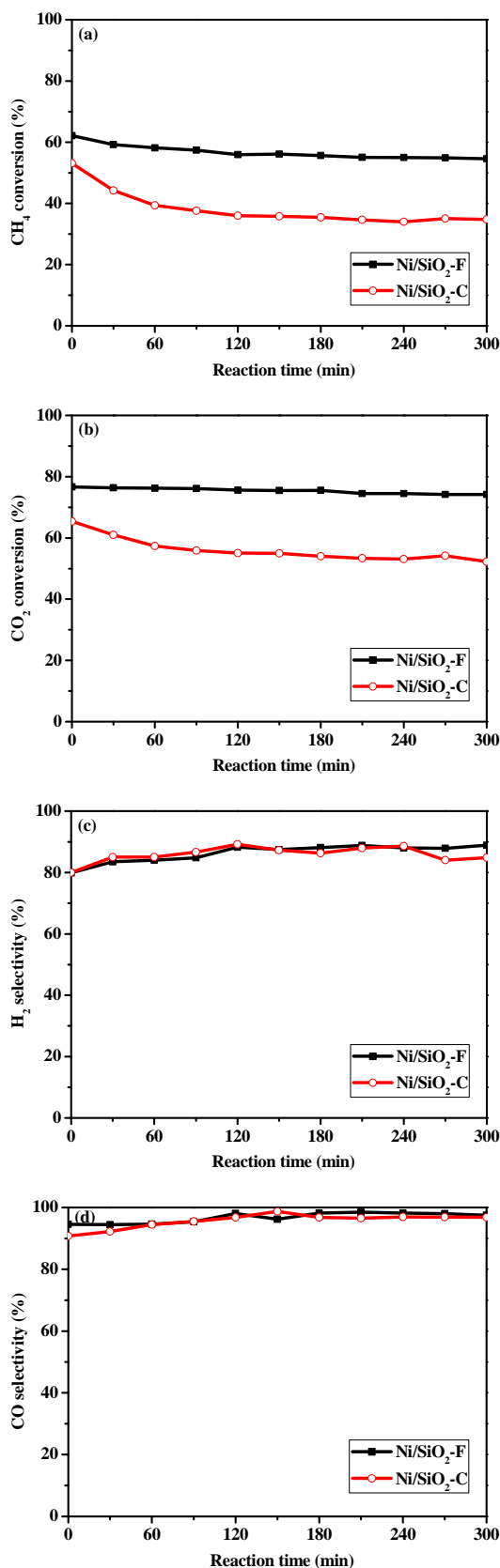


Fig. 5 Catalytic performances of Ni/SiO₂-F and Ni/SiO₂-C catalysts. Reaction conditions: P= 1 atm; T=700 °C; the nickel amount=10 wt%; CH₄:CO₂:Ar=1:1:2; GHSV=48 000 ml (h gcat)⁻¹.

Catalytic study.

Fig. 5 compares the catalytic performances between Ni/SiO₂-F and Ni/SiO₂-C catalysts as a function of reaction time. Both of the tested catalysts exhibited excellent catalytic activity under the current conditions. The conversion of CO₂ was always higher than that of methane, due to the occurrence of reverse water gas shift reaction.^{31,32} In comparison, Fig. 5a and 5b clearly shows that the Ni/SiO₂-F catalyst exhibited slightly higher initial activity and much better stability than the Ni/SiO₂-C counterpart. Besides, similar H₂ and CO selectivity was observed in Fig. 5c and 5d.

To interpret the different catalytic performances observed over Ni/SiO₂-F and Ni/SiO₂-C catalysts, a series of characterizations have been carried out. Shown in Fig. 6 are XRD patterns of Ni/SiO₂-F and Ni/SiO₂-C catalysts before and after reactions. Before reactions (Fig. 6a and Fig. 6b), only metallic Ni phase (JCPDS No. 04-0850) was identified for both of the catalysts. According to Scherrer equation, the average crystalline size of Ni on the fresh Ni/SiO₂-F and fresh Ni/SiO₂-C catalysts was calculated to be 8.2 and 18.7 nm, respectively. The electrospun Ni catalyst exhibited improved dispersion of the active phase. After reactions (Fig. 6c and 6d), a new phase corresponding to carbon (JCPDS No. 03-0053) was detected, due to carbon deposition during the reactions. Besides, the peak of carbon phase on the spent Ni/SiO₂-C catalyst was more intense than that on the spent Ni/SiO₂-F catalyst, suggesting more carbon deposition on the spent Ni/SiO₂-C catalyst. According to Scherrer equation, the average crystalline size of Ni on the spent Ni/SiO₂-F and Ni/SiO₂-C catalysts was calculated to be 8.4 and 18.8 nm, respectively. By comparing the particle size of Ni before and after reactions, it is concluded that sintering is insignificant in either Ni/SiO₂-F or Ni/SiO₂-C catalyst during the reactions.

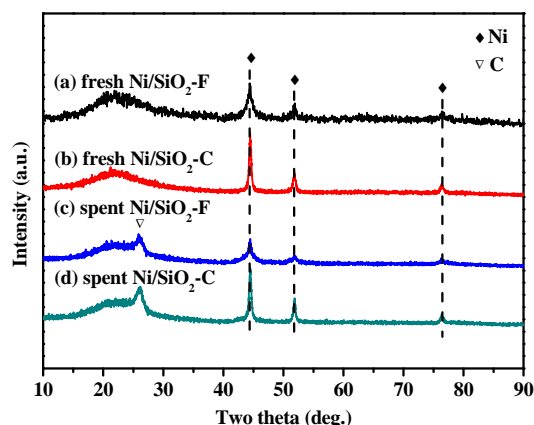


Fig. 6 XRD patterns of Ni/SiO₂-F and Ni/SiO₂-C catalysts before and after reactions: (a) fresh Ni/SiO₂-F catalyst; (b) fresh Ni/SiO₂-C catalyst; (c) spent Ni/SiO₂-F catalyst after reaction of 360 min; (d) spent Ni/SiO₂-C catalyst after reaction of 360 min.

HR-TEM images in Fig. 7 further confirmed XRD results. To discriminate the tiny black dots observed in Fig. 7a, STEM characterization was performed. Fig. S3 definitely reveals that the tiny black dots corresponded to the highly dispersed Ni nanoparticles. Furthermore, HR-TEM image of the cross-section of the nanofibers in Fig. S4 demonstrates that the Ni nanoparticles were uniformly confined inside the electrospun SiO₂ nanofibers. That is, most of the Ni particles were well confined inside the nanofibre of the fresh Ni/SiO₂-F catalyst. In the meantime, a few relatively large particles were also noticed

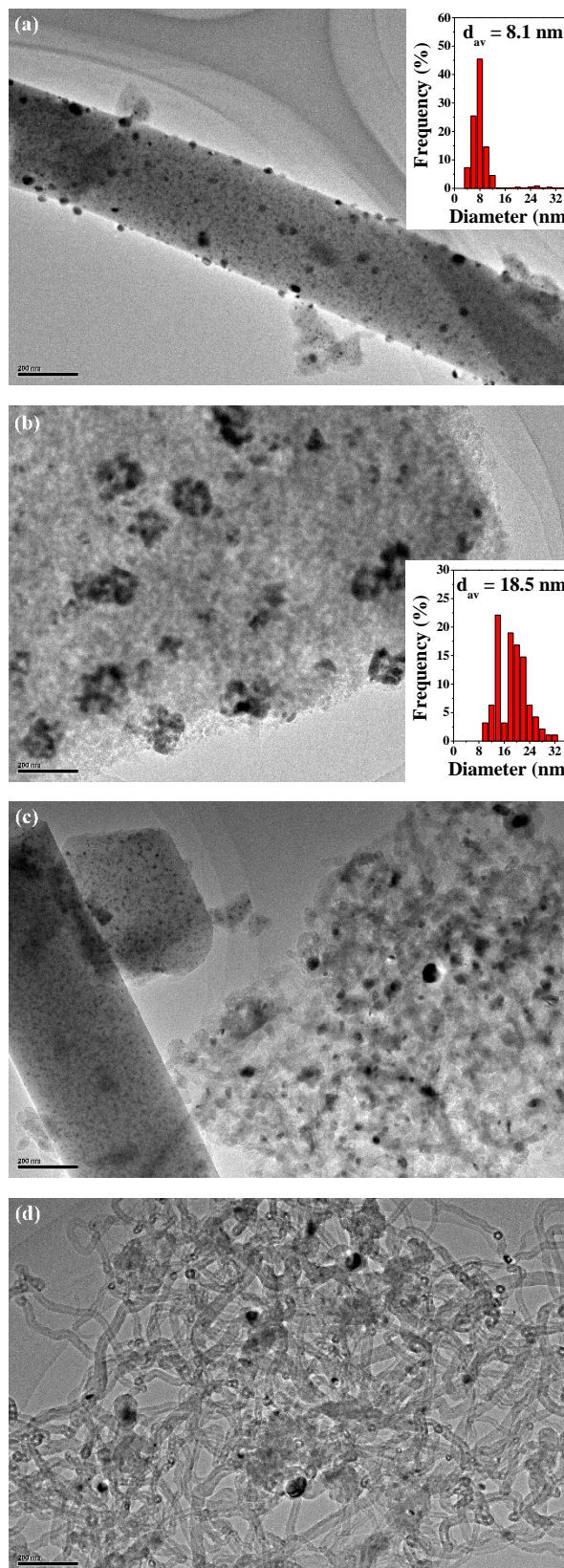


Fig. 7 HR-TEM images of Ni/SiO₂-F and Ni/SiO₂-C catalysts before and after reactions: (a) fresh Ni/SiO₂-F catalyst; (b) fresh Ni/SiO₂-C catalyst; (c) spent Ni/SiO₂-F catalyst after reaction of 360 min; (d) spent Ni/SiO₂-C catalyst after reaction of 360 min.

on the surface of the nanofibre. Much wider size distribution of Ni nanoparticles was observed on the fresh Ni/SiO₂-C catalyst (Fig. 7b). The average particle size of Ni in Fig. 7a and 7b was determined to be 8.1 and 18.5 nm respectively, in excellent agreement with that estimated by Sherrer equation in XRD characterization. By comparing Fig. 7a with 7c and Fig. 7b with 7d, respectively, it is concluded that little sintering of Ni nanoparticles occurred during the catalytic reactions. On the other hand, carbon deposition was observed on both the spent Ni/SiO₂-F catalyst (Fig. 7c) and the spent Ni/SiO₂-C catalyst (Fig. 7d). The carbon deposition on the spent Ni/SiO₂-C catalyst was much more severe than that on the spent Ni/SiO₂-F catalyst, consistent with the aforementioned XRD characterizations. Besides, SEM images of the spent Ni/SiO₂-F and Ni/SiO₂-C catalysts in Fig. S5 provide further support.

To further analyze the carbon deposition on the spent Ni/SiO₂-F and Ni/SiO₂-C catalysts, TG/DTA measurements were performed. TG curves in Fig. 8a clearly demonstrates that the carbon deposition on the Ni/SiO₂-F catalyst was dramatically inhibited. Fig. 8b indicates that three kinds of carbonaceous species were formed on the Ni/SiO₂-C catalyst, in agreement with the data reported in the literature.^{33,34} In contrast, only two kinds of carbonaceous species were detected on the Ni/SiO₂-F catalyst. Moreover, DTA peaks of the Ni/SiO₂-F catalyst shifted to lower temperature compared with those of the Ni/SiO₂-C counterpart, suggesting that the formed carbonaceous species on the Ni/SiO₂-F catalyst was more reactive. Both TG and DTA results demonstrate that the catalyst prepared by the electrospinning method is more resistant to carbon deposition.

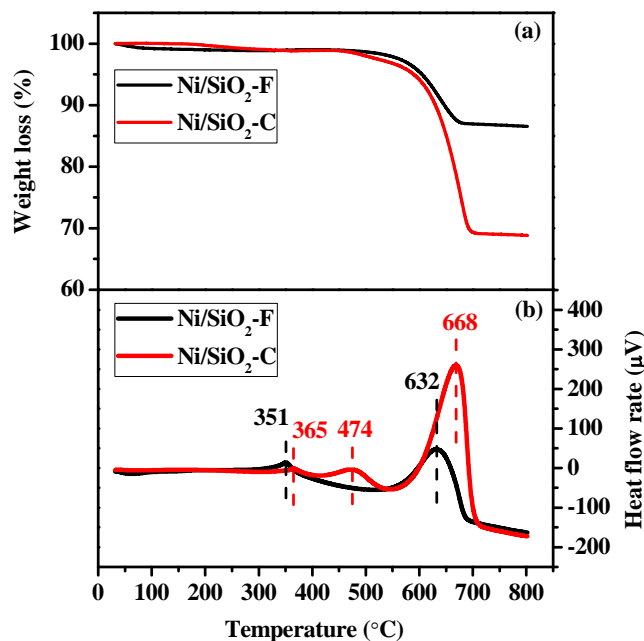


Fig. 8 TG (a) and DTA (b) profiles of the spent Ni/SiO₂-F and Ni/SiO₂-C catalysts after reaction of 360 min.

To confirm the TG/DTA results, O₂-TPO characterizations were carried out. Shown in Fig. 9 are O₂-TPO profiles of the spent Ni/SiO₂-F and Ni/SiO₂-C catalysts in which the intensity of the CO₂ signal represents the amount of carbon deposition. Firstly, the amount of carbon deposition on the Ni/SiO₂-F catalyst was much less than that on the Ni/SiO₂-C catalyst, in excellent agreement with TG curves. Secondly, three kinds of

carbonaceous species (C_α, C_β and C_γ) were observed on the Ni/SiO₂-C catalyst while only two kinds of carbonaceous species (C_α and C_γ) were detected on the Ni/SiO₂-F catalyst, consistent with DTA peaks. Based on the literature^{8,18,33,34}, the C_α species with O₂-TPO peak around 320 °C was ascribed to the amorphous carbon on the Ni sites which is responsible for the formation of synthesis gas. The C_β species with O₂-TPO peak around 445 °C was attributed to graphitic carbon, which is ascribed as the main reason for catalytic deactivation. The C_γ species with O₂-TPO peak around 647 °C corresponded to the carbon nanotubes. The absence of C_β species on the Ni/SiO₂-F catalyst suggests that the formation of graphitic carbon was greatly inhibited on the electrospinning prepared catalyst.

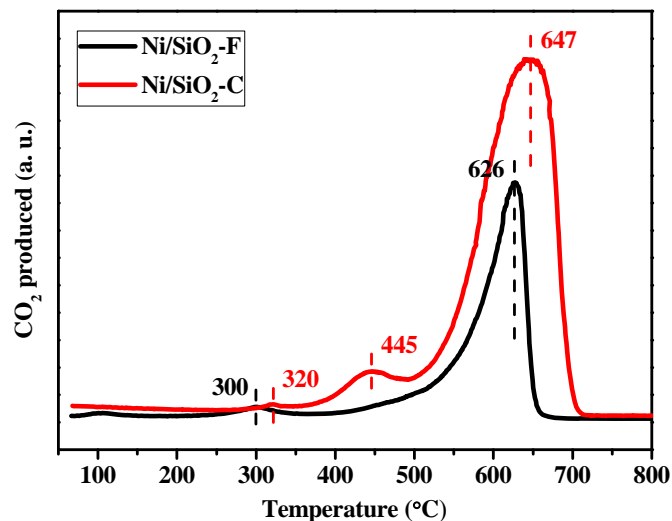


Fig. 9 O₂-TPO profiles of the spent Ni/SiO₂-F and Ni/SiO₂-C catalysts after reaction of 360 min.

General discussions.

The present work clearly demonstrates that SiO₂ nanofibre confined Ni catalyst prepared by the electrospinning technique possesses superior activity and stability in CO₂ reforming of methane (Fig. 5). It has been generally acknowledged that activity of the Ni-based catalyst depends critically on the dispersion of active metal.^{5,6} The catalyst with diminished Ni particle size always provides better activity. In the present work, both XRD (Fig. 6) and HR-TEM (Fig. 7) results prove that the Ni/SiO₂-F catalyst displayed improved dispersion than the Ni/SiO₂-C counterpart, which may rationalize the observed activity data. Besides, it has been widely accepted that carbon deposition and metal sintering are two main reasons for the deactivation of Ni-based catalyst in CO₂ reforming of methane.^{5,6} However, XRD (Fig. 6) and HR-TEM (Fig. 7) results revealed that metal sintering was insignificant and carbon deposition should be the main cause for the deactivation under the current conditions. TG/DTA (Fig. 8) and O₂-TPO (Fig. 9) profiles presented further evidence for the carbon deposition.

To understand the carbon deposition phenomena, the HR-TEM images of the spent Ni/SiO₂-F catalyst (Fig. 7c) and the spent Ni/SiO₂-C catalyst (Fig. 7d) were carefully examined and compared. It is noticed that, for the Ni/SiO₂-F catalyst (Fig. 7c), carbon deposition only occurred on the Ni nanoparticles with relatively large size locating on the surface of the SiO₂ nanofibre. The tiny Ni nanoparticles confined inside the SiO₂ nanofibre

remained intact towards carbon deposition. Namely, little carbon nanofibre was observed on the confined tiny Ni nanoparticles. On the other hand, for the Ni/SiO₂-C catalyst (Fig. 7d), carbon deposition occurred extensively on all of the Ni nanoparticles. These results clearly suggest the confinement effect induced by the nanofibre in the Ni/SiO₂-F catalyst.

Furthermore, the confinement effect of the Ni/SiO₂-F catalyst can be directly verified by H₂-TPR characterization. Fig. 10 compares the H₂-TPR profiles between Ni/SiO₂-F and Ni/SiO₂-C catalysts. For the Ni/SiO₂-C catalyst, two reduction peaks were observed at temperature of 399 and 451 °C. Based on the literature³⁵⁻³⁷, the peak with lower temperature corresponds to the reduction of NiO that interacts weakly with SiO₂ while the one with higher temperature is from the reduction of NiO that interacts strongly with SiO₂. In the meantime, two reduction peaks located at 399 and 702 °C were observed for the Ni/SiO₂-F catalyst. In comparison, a remarkable shift of the reduction peak with higher temperature from 451 °C in the Ni/SiO₂-C catalyst to 702 °C in the Ni/SiO₂-F catalyst was observed. Moreover, the proportion of the reduction peak at higher temperature was significantly increased in the Ni/SiO₂-F catalyst compared with that in the Ni/SiO₂-C counterpart. H₂-TPR results suggest that a much stronger interaction between metal and support exists in the Ni/SiO₂-F catalyst.³⁸

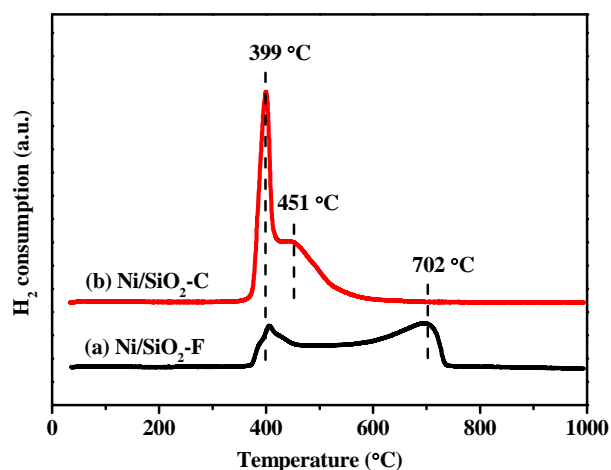


Fig. 10 H₂-TPR profiles of (a) Ni/SiO₂-F and Ni/SiO₂-C catalysts.

In addition, the information of the basic sites in the catalysts was characterized with CO₂-TPD measurements. As shown in Fig. 11, both Ni/SiO₂-F and Ni/SiO₂-C catalysts exhibited one broad peak from 150 to 700 °C, suggesting weak basic sites.^{17,18} In comparison, the Ni/SiO₂-F catalyst possessed almost twice amount of basic sites as the Ni/SiO₂-C counterpart. The increased adsorption of CO₂ molecules is supposed to provide more oxygen species on the surface of the catalysts, which should benefit the gasification of intermediate carbon and thus improve the coke-resistance of the catalyst.^{17,18} Synthesis of SiO₂ nanofibre confined Ni catalyst by the electrospinning technique resulted in catalyst with improved metal dispersion, enhanced metal-support interaction and more abundant basic

sites, leading to superior catalytic performances in CO₂ reforming of methane.

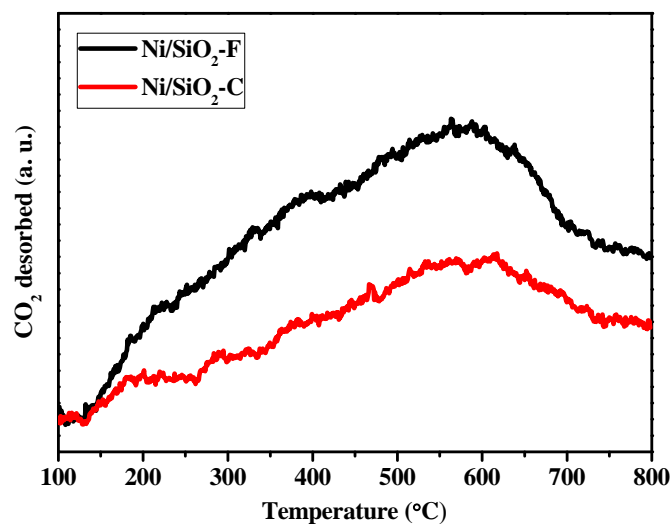


Fig. 11 CO₂-TPD profiles of (a) Ni/SiO₂-F and Ni/SiO₂-C catalysts.

Moreover, the Ni/SiO₂-F catalyst was compared with the Ni/SiO₂-FI catalyst to examine the morphology effect of the support. As shown in Fig. S6, the Ni/SiO₂-FI catalyst had a much lower activity than the Ni/SiO₂-F counterpart (Fig. 5). HR-TEM characterization (Fig. S7) reveals that the Ni/SiO₂-FI catalyst had a much lower Ni dispersion than the Ni/SiO₂-F counterpart (Fig. 7a), rationalizing the much poorer activity observed on the Ni/SiO₂-FI catalyst. Therefore, the superior catalyst performance obtained on the Ni/SiO₂-F catalyst should not result from the morphology effect of the support.

For the Ni/SiO₂-F catalyst, TOF (turnover frequency), defined as CH₄ conversion per surface Ni atom per second, was calculated by estimating Ni dispersion from $D\% = 100/d_{\text{TEM}}$.³⁹ TOF of the Ni/SiO₂-F catalyst at 30 min was calculated as 0.43 s⁻¹. TOF values on Ni/SiO₂ catalysts at similar reaction temperature were reported to vary from 0.31 to 182 s⁻¹, depending on the Ni particle size, the metal-support interaction and other reaction conditions.^{40,41} In the present work, the obtained TOF value is in the range reported by the literature.

Besides, the Ni/SiO₂-F catalyst was evaluated with a prolonged reaction time. As shown in Fig. S8, excellent stability was observed. It has been generally accepted that coke formation on Ni surface initiates at the Ni step edges where carbon atoms nucleate and grow into graphene sheets.^{42,43} The catalyst gradually deactivates as the graphene layers continuously encapsulate the Ni particles. Therefore, to further circumvent coke deposition and improve the catalytic stability to a greater degree, appropriate promoters should be added to the Ni/SiO₂-F catalyst.

Conclusions

SiO₂ nanofibre confined Ni catalyst has been successfully synthesized by the electrospinning technique for CO₂ reforming of methane. The catalyst was characterized with TG/DTA, XPS,

N₂ sorption, XRD, SEM, HR-TEM, O₂-TPO, H₂-TPR and CO₂-TPD measurements. The obtained results suggested 800 °C as the optimal calcination temperature. Compared with the conventionally prepared catalyst using commercial SiO₂ powder as the support, the electrospinning synthesized Ni/SiO₂ nanofibre catalyst exhibited slightly higher initial activity and much better stability. The slightly higher activity was ascribed to the improved dispersion of Ni and the much better stability was due to significantly alleviated carbon deposition. SiO₂ nanofibre confined Ni catalyst possessed much stronger metal-support interaction and more abundant basic sites, leading to enhanced coke-resistance property. It is expected that this simple, versatile, cheap and effective method will be promising as a general and scalable technique for the synthesis of nanoconfined catalysts with superior activity and stability.

Acknowledgements

We acknowledge with pleasure the financial support of this work by the National Natural Science Foundation of China (No. 21403012 and No. 51103005), Beijing Natural Science Foundation (No. 2144053), the Fundamental Research Funds for the Central Universities (No. ZY1404, No. JD1407 and No. JD1513), the Beijing Higher Education Young Elite Teacher Project (No. YETP0493), and the Program of Beijing Excellent Talents (No. 2013D009016000003).

Notes and references

^a State Key Laboratory of Chemical Resource Engineering, Beijing University of Chemical Technology, 15 Beisanhuan East Road, P.O. Box 266, Chaoyang District, Beijing 100029, P.R. China. E-mail: wangzj@mail.buct.edu.cn; Tel./Fax: +86 10 64437983.

^b State Key Laboratory of Organic-Inorganic Composites, Beijing University of Chemical Technology, 15 Beisanhuan East Road, P.O. Box 266, Chaoyang District, Beijing 100029, P.R. China.

† Electronic Supplementary Information (ESI) available: XPS spectra, SEM, HR-TEM and STEM images, catalytic performances. See DOI: 10.1039/b000000x/

- 1 C.-j. Liu, U. Burghaus, F. Besenbacher and Z. L. Wang, *ACS Nano.*, 2010, **4**, 5517.
- 2 D. P. Serrano, J. M. Coronado, V. A. de la Peña O'Shea, P. Pizarro and J. Á. Botas, *J. Mater. Chem. A*, 2013, **1**, 12016.
- 3 C. Federsel, R. Jackstell and M. Beller, *Angew. Chem. Int. Ed.*, 2010, **49**, 6254.
- 4 D. Pakhare and J. Spivey, *Chem. Soc. Rev.*, 2014, **43**, 7813.
- 5 M. Tang, L. Xu and M. Fan, *Int. J. Hydrogen Energy*, 2014, **39**, 15482.
- 6 C.-j. Liu, J. Ye, J. Jiang and Y. Pan, *ChemCatChem.*, 2011, **3**, 529.
- 7 X. Xie, T. Otremba, P. Littlewood, R. Schomäcker and A. Thomas, *ACS Catal.*, 2013, **3**, 224.
- 8 X. Du, D. Zhang, L. Shi, R. Gao and J. Zhang, *J. Phys. Chem. C*, 2012, **116**, 10009.
- 9 I. O. Costilla, M. D. Sánchez and C. E. Gigola, *Appl. Catal. A*, 2014, **478**, 38.
- 10 X. Pan and X. Bao, *Acc. Chem. Res.*, 2011, **44**, 553.
- 11 Q. Fu, F. Yang and X. Bao, *Acc. Chem. Res.*, 2013, **46**, 1692.
- 12 S. Li and J. Gong, *Chem. Soc. Rev.*, 2014, **43**, 7245.
- 13 G. Prieto, J. Zečević, H. Fredrich, K. P. de Jong and P. E. de Jongh, *Nat. Mater.*, 2012, **12**, 34.
- 14 S. He, Z. An, M. Wei, D. G. Evans and X. Duan, *Chem. Commun.*, 2013, **49**, 5912.
- 15 C. Zhang, W. Zhu, S. Li, G. Wu, X. Ma, X. Wang and J. Gong, *Chem. Commun.*, 2013, **49**, 9383.
- 16 T. Xie, L. Shi, J. Zhang and D. Zhang, *Chem. Commun.*, 2014, **50**, 7250.
- 17 X. Du, D. Zhang, R. Gao, L. Huang, L. Shi and J. Zhang, *Chem. Commun.*, 2013, **49**, 6770.
- 18 X. Du, D. Zhang, L. Shi, R. Gao and J. Zhang, *Nanoscale*, 2013, **5**, 2659.
- 19 C.-L. Zhang and S.-H. Yu, *Chem. Soc. Rev.*, 2014, **43**, 4423.
- 20 S. Cavaliere, S. Subianto, I. Savych, D. J. Jones and J. Roziere, *Energy Environ. Sci.*, 2011, **4**, 4761.
- 21 R. A. Naphade, M. Tathavadekar, J. P. Jog, S. Agarkar and S. Ogale, *J. Mater. Chem. A*, 2014, **2**, 975.
- 22 S. Abouali, M. A. Garakani, B. Zhang, H. Luo, Z.-L. Xu, J.-Q. Huang, J. Huang and J.-K. Kim, *J. Mater. Chem. A*, 2014, **2**, 16939.
- 23 J. Xiang, J. Li, X. Zhang, Q. Ye, J. Xu and X. Shen, *J. Mater. Chem. A*, 2014, **2**, 16905.
- 24 N. T. Hieu, J. Suk, D. W. Kim, J. S. Park and Y. Kang, *J. Mater. Chem. A*, 2014, **2**, 15094.
- 25 Y. Wang, G. Han, Y. Li, M. Li and J. Wu, *J. Mater. Chem. A*, 2014, **2**, 16856.
- 26 S. Wen, L. Liu, L. Zhang, Q. Chen, L. Zhang and H. Fong, *Mater. Lett.*, 2010, **64**, 1517.
- 27 Z.-j. Wang, Y. Zhao, L. Cui, H. Du, P. Yao and C.-j. Liu, *Green Chem.*, 2007, **9**, 554.
- 28 Y. Zhao, H. Wang, X. Lu, X. Li, Y. Yang and C. Wang, *Mater. Lett.*, 2008, **62**, 143.
- 29 X. Wang, H. Fan, P. Ren, H. Yu and J. Li, *Mater. Res. Bull.*, 2012, **47**, 1734.
- 30 C. D. Wagner, W. M. Riggs, L. E. Davis, J. F. Moulder and G. E. Mullenberg, in *Handbook of X-ray Photoelectron Spectroscopy*, Perkin-Elmer, Minnesota, 1979.
- 31 X. Zhu, P. Huo, Y.-p. Zhang, D.-g. Cheng and C.-j. Liu, *Appl. Catal. B*, 2008, **81**, 132.
- 32 M. C. J. Bradford and M. A. Vannice, *Appl. Catal. A*, 1996, **142**, 73.
- 33 D.-g. Cheng, X. Zhu, Y. Ben, F. He, L. Cui and C.-j. Liu, *Catal. Today*, 2006, **115**, 205.
- 34 Z. L. Zhang and X. E. Verykios, *Catal. Today*, 1994, **21**, 589.
- 35 Y.-x. Pan, C.-j. Liu and P. Shi, *J. Power Sources*, 2008, **176**, 46.
- 36 S. Tomiyama, R. Takahashi, S. Sato, T. Sodesawa and S. Yoshida, *Appl. Catal. A*, 2003, **241**, 349.
- 37 M. Che, Z. X. Cheng and C. Louis, *J. Am. Chem. Soc.*, 1995, **117**, 2008.
- 38 Z.-j. Wang, Y. Liu, P. Shi, C.-j. Liu and Y. Liu, *Appl. Catal. B*, 2009, **90**, 570.
- 39 J. Wei and E. Iglesia, *J. Catal.*, 2004, **224**, 370.
- 40 X. Zhu, Y.-p. Zhang and C.-j. Liu, *Catal. Lett.*, 2007, **118**, 306.
- 41 J. Zhang and F. Li, *Appl. Catal. B*, 2015, **176**, 513.
- 42 S. Helveg, C. López-Cartes, J. Sehested, P. L. Hansen, B. S. Clausen, J. R. Rostrup-Nielsen, F. Abid-Pedersen and J. K. Nørskov, *Nature*, 2004, **427**, 426.
- 43 H. S. Bengaard, J. K. Nørskov, J. Sehested, B. S. Clausen, L. P. Nielsen, A. M. Molenbroek and J. R. Rostrup-Nielsen, *J. Catal.*, 2002, **209**, 365.